Design of Surface Shape Control for Large Two-Dimensional Arrays

Gunter Stein, *Fellow, IEEE* and Dimitry Gorinevsky, *Senior Member, IEEE,*

***Abstract*— This work develops control design technology for active shape control of reflective surfaces using large spatially distributed actuator arrays. The potential applications are in astronomy, adaptive optic, beam control, space-based imaging, and other optics and imaging applications. In a very large lightweight active reflector, surface shape (figure) might be controlled by an array of actuators and sensors that counts millions of cells. The control technology discussed in this paper is scalable to these large array dimensions. This paper develops a classically-motivated design methodology for distributed localized control laws of very large actuator/sensor arrays. The methodology uses standard PI-compensation, plus lags and/or notch-filters, to deal with temporal dynamics in each actuator channel. It achieves scalability to very large array sizes by imposing spatially localized fixed-form constraints on the control law structure. In this setup, the entire spatial-temporal design model can be transformed, via Laplace transforms in time and 2-D discrete Fourier transforms in space, to produce a family of dynamic systems whose closed loop characteristics can be subjected to standard classical control-engineering specifications, including stability, performance, and robustness. These specifications can be satisfied for all members of the family by solving linear programs to find parameters of the fixed-form structure. The veracity of this methodology is illustrated with a design example loosely resembling an actively controlled reflector whose local deformations are controlled by a hexagonal array of actuator/sensor cells.**

***Index Terms*— active reflector control, multidimensional system, distributed systems, control design**

I. Introduction

THIS work develops control design technology for active shape control of reflective surfaces using large spatially distributed actuator arrays. The potential applications are in astronomy, adaptive optics, and space areas. Reflectors with actuators that help to attain and hold a given shape are usually known as ‘active’ reflectors. These require setpoint control. Unlike that, ‘adaptive’ mirrors are continuosely changing their shape to counter atmospheric disturbances. This requires servo control. Practical design of low-bandwidth servo control is the same as setpoint control design and these are not distinguished in this paper.

In a large reflector, surface shape (figure) is controlled by an array of actuators and sensors that might count millions of cells. The control technology discussed in this paper is scalable to these large array dimensions. One application area where large active mirror surfaces would be required is for space born instruments: optical, infrared, or radio frequency. Very large lightweight space reflectors must have low areal density, and they must be deployable to limit launch volume. They are subject to initial deployment errors and figure distortions, such as caused by thermal disturbances. Thus, there is a need and many on-going efforts to develop active reflectors as “smart structures”. The mirror surface shape (figure) of such reflectors is controlled by an array of actuator/sensor cells that measure and compensate distortions. Large reflectors with fine granularity may need millions of such cells.

A concept for active space reflectors described in [6] envisions special membranes attached to the reflector surface with integrated actuators, sensors, and computing elements. Plastic micro-electro-mechanical system (MEMS) actuators embedded in the membrane would be distributed on a regular hexagonal grid. Each cell of the grid would have a collocated local deformation sensor and a computing element controlling the actuator. The figure control approach would perform most of the computations for each actuator locally, using information from near neighbors only. The architecture requires neighbor-to-neighbor communication only and is scalable to extremely large numbers of cells, irrespective of the specific design of actuators, cell grid patterns, sensors, and computing/communication platforms.

In addition to active primary reflectors, the distributed localized control technology discussed in this paper is also applicable to deformable mirrors elsewhere in the optical path. Deformable mirrors in active or adaptive optics systems are used for conjugating wavefront to correct disturbances caused by mis-figured primary mirrors or by atmospheric turbulence. Current deformable mirrors use piezoelectric or electrostatic actuators with up to 100,000 elements. There is also a significant effort to develop deformable mirrors based on MEMS technology. Such mirrors will be relatively small, and they may have millions of actuators to enable mega-pixel resolution images.

Deformable mirrors in adaptive optics systems are usually controlled with a centralized computer using sparse matrix inversion techniques. Decentralized localized control approaches will significantly improve computational performance, and for MEMS technology, they could be implemented on the same silicon substrate as the actuator. A description of an experimenal MEMS adaptive optics system with distributed local computing can be found in [12].

While localized control architectures can be easily understood and explained, the design of scalable distributed control laws for such architectures is a more difficult engineering task. It is not covered by existing control technologies. The purpose of this work is to develop and demonstrate design methods for this task, applicable to two-dimensional (2-D)

Honeywell Laboratoriess, Minneapolis, MN 55418
Honeywell Laboratories, Fremont, CA 94539; gorinevsky@ieee.org, dimitry. gorinevsky@honeywell.com

arrays, and based on explicit engineering specifications. The usual requirements of performance, robustness, and actuator range are considered with an emphasis on spatial frequency domain properties of the control loop. The systematic control design and analysis approach in this paper involves system performance parameters and can be used as an integral part of system trade studies when designing large-scale actively controlled reflectors. The models and parts of the control design problem formulation in this paper are related to these in [10], [7], where some more references to the telescope applications can be found. The design and analysis approach herein is however different.

Mathematical approaches to analysis and design of feedback control of large distributed systems with regular array structure are proposed and explored in a number of publications. The most relevant to the topic of this paper are [1], [2], [3], [4], [10], where further references can be found. Most of the cited work is concerned with formal mathematical feedback control design in the spirit of the modern-control era. In this work, we approach the design problem from a more classical and practical perspective. Temporal loops are taken to be simple PI-structures, augmented with high-frequency compensation to handle resonant flexible dynamics. These controller structures are appropriate for many, if not most, practical situations. We achieve scalability to large array sizes by imposing distributed local control as a fixed-form constraint on the spatial control structure. Linear programs (LPs) are then used to find parameters for the fixed-form structure that satisfy explicit engineering specifications. Conceptually, this approach follows the work in [5]. It extends that work to two spatial dimensions, it adds additional considerations of dynamical bandwidth, and it also expands the list of engineering specifications. In particular, this paper explicitly adds modeling error robustness to the specifications and incorporates these into the LP optimization framework .

An approach closely related to ours is spatial loop-shaping (or tuning) of distributed controllers, as discussed in [8], [9]. This approach was successfully applied to industrial process control (paper machine) applications with hundreds of actuators. Like the approach in this paper, spatial loop-shaping accommodates many important engineering specifications for control design. The localized controllers in [8], [9] are obtained by truncating non-localized controllers. Herein, optimized localized controllers are synthesized directly.

II. System Models for Two-Dimensional Arrays

As described above, the systems under consideration in this paper consist of large arrays of actuators and sensors, arranged so that they can collectively deform a surface in order to achieve desired nominal shapes, or to correct shape imperfections, and/or to counter dynamic disturbances. Mathematical models for these systems are described below.

We assume that each actuator, when displaced individually, creates a static (steady state) surface deformation called an actuator influence function, designated by $h_k(x-x_k, y-y_k)$. Here the index k references a specific actuator, h_k is the actuator's surface deformation caused by a unit displacement, x, y are spatial coordinates of the surface, and x_k, y_k describe the actuator's location. We further assume that the surface deformation mechanism is linear, so that total deformations are sums of deformations created by individual actuators, i.e.

$$d(x,y) = \sum_{k=1}^{N} h_k(x-x_k,\ y-y_k)\ u_k, \tag{1}$$

where $d(x,y)$ is the total surface deformation, N is the total number of actuators, and u_k are individual actuator displacements.

Of course, the actuator influence functions $h_k(x-x_k, y-y_k)$ in (1) depend on the membrane material, thickness, attachement to actuators, and its other physical properties. Bending stiffness and tension of the membrane mean that the deformation of one cell influences the deformation of another. This paper describes the influence empirically by functions $h_k(x-x_k, y-y_k)$ without getting into the mechanical design detail.

Each actuator has an associated sensor that measures either the precise deformation of the surface at location x_k, y_k or its weighted spatial average in a neighborhood of x_k, y_k. The latter situation is generally preferred because it helps to alleviate spatial-aliasing phenomena in the sensing system. In either case, the sensed outputs can be written as ($l = 1, 2, \ldots, N$)

$$d_l = d\,(x_l, y_l) = \sum_{k=1}^{N} h_k(x_l-x_k,\ y_l-y_k)\ u_k, \tag{2}$$

where d and h_k correspond either directly to their counterparts in Eqn (1), or they correspond to weighted spatial averages, as defined by the sensors' design. We will use the same symbols for both cases. Of course, Eqn (2) can be expressed in the more compact vector-matrix notation,

$$d \ = \ H\,u \tag{3}$$

with N-vector $d = \{d_l\}$, N-vector $u = \{u_k\}$, and $N \times N$-matrix $H = \{h_k(x_l - x_k, y_l - y_k)\}$. The detailed structure of matrix H is determined by the specific ordering scheme used to index individual cells in the array.

Equation (3) defines steady state deformations measured by all sensors due to known displacements of all actuators. Such a steady-state model is commonly used in design of adaptive optics systems and assumes that the actuator authority is sufficient to overpower the dynamics of the deformed surface. This assumption might become less valid for very large scale actuator arrays, where each actuator is less powerful. In that case, the deformations d in (3) do not appear instantaneously. Rather, they experience dynamic evolutions in response to actuator displacement commands. Such dynamics are associated with the surface itself (e.g., distributed mass and stiffness producing damped resonances), with the response of actuators to commands (e.g., spring-mass and/or RLC circuit lags), and with dynamic elements deliberately introduced in the control law (e.g., integral action).

For purposes of this paper, we will assume that dynamic responses of surface deformation can be characterized by

temporal frequency responses such as those shown in Figure 1A. They consist of flat (steady state) responses at low frequencies, followed by a series of resonances at higher frequencies corresponding to actuator dynamics and resonance modes of the surface. These characteristics represent a broad class of surface control problems. In particular, detailed partial differential equation models and their finite element approximations exhibit them naturally.

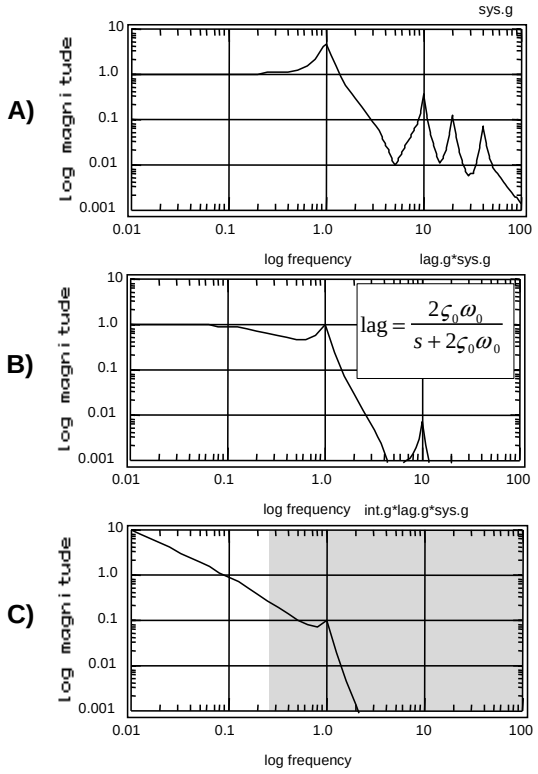

Fig. 1. Surface Deformation Dynamics. A) Typical Temporal Frequency Response of h_{mn}; B) Response with Lag Compensation To Suppress Resonances; C) Response with Lag Compensation and Integral Action

Key parameters of these responses are their DC gains h_{lk}, their resonance frequencies $\omega_0, \omega_1 \ldots$, and their damping ratios $\varsigma_0, \varsigma_1 \ldots$ specifying the height of resonance peaks. While much academic research has been done to attempt high bandwidth control of such resonant systems (e.g., crossover frequencies $\omega_c > \omega_0$), more pragmatic control design practice calls for crossover below ω_0. Lag compensation and/or notch-filter compensation is used to suppress resonance peaks (as illustrated in Figure 1B), and integral action is used to raise low frequency loop gains (Figure 1C). A 'rule of thumb' for maximum achievable crossover frequencies with this design practice is $\omega_c \approx 0.5\varsigma_0\omega_0$.

Following such pragmatic design, we will assume that temporal control compensation consists of identical lag- and/or notch-filters in each sensor channel plus integral action, modified by small amounts of 'integrator leakage'. These assumptions yield the following approximate spatial-temporal deformation model, valid for all temporal frequencies $\omega < 0.5\varsigma_0\omega_0$:

$$\begin{aligned} \frac{du}{dt} &= -Au + u_{cmd} \\ d &= Hu + d_0 \end{aligned} \tag{4}$$

In this model, the $N \times N$-matrix A represents integrator leakage. Its nominal value will be $A = 0$, corresponding to pure integral action. However, some deformation matrices H will require A to be non-zero in order to construct averages of u over spatial neighborhoods to maintain stability in the presence of small gains in certain spatial directions of H. This will be discussed in more detail later. Also, the term d_0 represents external disturbances creating undesired surface deformations to be compensated via active control.

On first inspection, the model in Eqn (4) is an ordinary multivariable dynamic system for which standard multivariable analysis/design techniques ought to provide adequate tools. In one way or another, these standard techniques are based on the principle of inversion, e.g., let

$$u_{cmd} = -\alpha H^x (d - r), \tag{5}$$

where scalar α is the desired temporal closed-loop bandwidth, H^x is an 'inverse' of matrix H (either full or approximate) and N-vector r is the desired (commanded) reference shape for the surface deformation.

Upon substituting this control law into (4), the closed- loop system becomes

$$\begin{aligned} \frac{du}{dt} &= -[A + \alpha\, H^x H]u + \alpha\, H^x (r - d_0) \\ d &= Hu + d_0 \end{aligned} \tag{6}$$

So, choosing $H^x = H^{-1}$ and setting $A = 0$ produces very nice closed-loop behavior:

$$\begin{aligned} \frac{du}{dt} &= -\alpha(u - H^{-1}(r - d_0)) \\ d &= Hu + d_0 \end{aligned} \tag{7}$$

Actuator displacements reach the steady state values $H^{-1}(r - d_0)$ with uniform temporal speeds-of-response (time constant $1/\alpha$), and surface deformations at all cells reach their desired steady state values $d = H(H^{-1}(r - d_0)) + d_0 = r$ in similarly nice fashion.

Of course, circumstances are never ideal. Real H-matrices are always uncertain. Often they are not even nominally invertible, or they are so ill-conditioned that their full inverses produce excessive actuator displacements, $H^{-1}(r - d_0)$. So, invariably, some form of approximate inverse must be used, possibly based on singular value decompositions, on regularization, or on modal decompositions. Unfortunately, these various approximations are increasingly difficult to calculate as array dimensions get very large (e.g., $N \approx 10^6$). Moreover, they are centralized, requiring all sensed signals to be communicated to a central processor and requiring its computed control commands to be communicated back to all actuators in hard-real-time. Today's software packages, communication architectures, and hardware elements have difficulty with such demands.

For these various reasons, it proves useful to take advantage of additional structure inherent in many large actuator/sensor arrays, namely

1) identical influence functions for each cell,

2) regular cell spacing along the coordinate axes, and
3) localized influence functions that cause significant non-zero deformations only in small neighborhoods, relative to the total extent of the array.

Actuator/sensor arrays with these features are called spatially invariant. They can be approximated as infinite in extent, and spatial transform methods can be applied to them in order to simplify plant description, control design, and control implementation [1], [3], [4], [5]. The needed concepts are briefly summarized below.

On an assumed infinite 2-D spatial domain, the continuous deformation function from Eqn (1) can be rewritten as

$$d(x,y) = \sum_{m=-\infty}^{\infty} \sum_{n=-\infty}^{\infty} h(x - m\,\Delta x,\ y - n\,\Delta y)\ u_{mn} \quad (8)$$

where we have taken advantage of the actuators' common influence function $h(x,y)$ and their regular spacing at locations $m\Delta x$, $n\Delta y$ along the coordinate axes. The single index k has been replaced by a double index m, n to reference individual cells on the uniform 2-D grid.

Equation (8) is a two-dimensional convolution of the continuous function $h(x,y)$ with the discrete sequence u_{mn}. Assuming that the function is integrable and the sequence summable, this convolution can be replaced by a product of transforms. Namely,

$$\tilde{d}(\xi,\lambda) \quad = \quad \tilde{h}(\xi,\lambda)u^*(v,w)\Big|_{v=\exp(j\xi\Delta x),\ w=\exp(j\lambda\Delta y)} \quad (9)$$

where $\tilde{d}(\xi,\lambda)$ and $\tilde{h}(\xi,\lambda)$ denote the continuous (Fourier) transforms of their respective functions, e.g., and $\hat{u}^*(v,w)$ denotes the discrete z transform of the sequence u_{mn}. In both cases, the variables ξ,λ represent spatial frequencies (e.g., radians/meter) along the spatial coordinates, so Eqn (9) can be interpreted as a description of the frequency content of the function $d(x,y)$ on the spatial domain.

While Eqn (8) and its transform (9) are the primary objects of interest for assessing effective control of surface deformations, the actual measurements available for control are limited to a spatially sampled version of these equations. The sampled equation corresponding to (2) is as follows

$$d_{op} = \sum_{m=-\infty}^{\infty} \sum_{n=-\infty}^{\infty} h((o-m)\Delta x,\ (p-n)\Delta y)\ u_{mn} \quad (10)$$

where $d_{op} = d(o\Delta x, p\Delta y)$ and $-\infty < o,p < \infty$. Corresponding discrete transform:

$$d^*(v,w) \quad = \quad h^*(v,w)\ u^*(v,w) \quad (11)$$

On an assumed infinite 2-D spatial domain, the controller structure implementing an integration with leakage in Eqn (4) takes the form

$$\left(\frac{du}{dt}\right)_{mn} \quad = \quad u_{cmd;mn} - \sum_{o=-\infty}^{\infty} \sum_{p=-\infty}^{\infty} a_{(m-o)\ (n-p)}\ u_{op} \quad (12)$$

Combining the spatial transforms (11) with a transform $a^*(v,w)$ computed for the kernel a_{mn} in the temporal controller structure (12) yields spatial-temporal transfer functions for the plant

$$\begin{aligned} s\,u^*(v,w) &= -a^*(v,w)\ u^*(v,w) + u^*_{cmd}(v,w) \\ d^*(v,w) &= h^*(v,w)\ u^*(v,w) + d^*_0(v,w) \\ &= \frac{h^*(v,w)}{s + a^*(v,w)} u^*_{cmd}(v,w) + d^*_0(v,w), \end{aligned} \quad (13)$$

where the complex variable s is the usual temporal (Laplace) transform for differentiation. Note that Eqn (13) describes a family of first order dynamic systems whose variables and parameters are indexed by the spatial frequencies v,w. In other words, each frequency component of surface deformation is governed by its own simple first order dynamic system!

Design methods for transform models (13) and (20) begin by adding the following fixed-form control law to (12):

$$(u_{cmd})_{mn} = -\sum_{o=-\infty}^{\infty} \sum_{p=-\infty}^{\infty} k_{(m-o)\ (n-p)}\ (d_{op} - r_{op}) \quad (14)$$

where k_{mn} is a discrete control influence function and r_{op} is the commanded reference shape. In what follows, we will use the frequency transform $k^*(v,w)$ of the kernel k_{mn}.

Control law (14) has been successfully applied in numerous practical 1-D control processes such as paper machines [8], [9]. It uses the control influence function to feed back local deformation errors $d_{op} - r_{op}$ from each actuator/sensor cell as well as other errors from a neighborhood around that cell. As long as k_{mn} is sufficiently localized (i.e., only a few layers of neighboring cells have non-zero gains), implementations of (14) can be spatially distributed and can therefore be scaled-up to very large array dimensions.

The observation enabling the design and analysis in this work is that whenever the kernels $\{h_{mn}\}$, $\{k_{mn}\}$, and $\{a_{mn}\}$, are symmetric (e.g., $h_{mn} = h_{-m-n},\ \forall\ m,n$), their transforms h^*, a^* and k^* are real-valued for spatial frequencies on the unit circle. This follows from the definition of (two-sided) discrete transforms. It is further assumed that h^*, a^* and k^* are indeed real-valued on the unit circle. Without a loss of the generality, it will be assumed that the gain h^* is positive at the frequencies where the system is controllable. The gain might be zero at some frequencies.

III. Model Uncertainties

We now have two different models of actuator/sensor arrays for surface deformation control. The first model is given by Eqn (4). It properly accommodates finite spatial domains, arbitrary cell locations, and different actuator influence functions across the array, as seen particularly near domain boundaries. This generality is purchased at the expense of the curse of dimensionality. The model's applications, for both analysis and control design, are restricted to modest array sizes.

The second model in give by Eqn (13). This model exploits spatial invariance and an (assumed) infinite spatial domain to approximate Eqn (4) as a family of first-order dynamic systems. As demonstrated later, this simplification enables analysis and design for arbitrarily large array sizes.

In the spirit of modern robust control, however, both models must be seen as nominal descriptions only, and a deliberate effort must be made to characterize their inherent uncertainties,

in the presence of which eventual control designs are expected to be robust.

For distributed actuator/sensor arrays, uncertainties are associated primarily with the sampled actuator influence functions in Eqn (2), i.e., $h_k(x_l - x_k, y_l - y_k)$. Even if these functions are nominally identical for each cell of the array, their actual shapes will differ from cell to cell because each cell is a separate physical instantiation. Hence, it is reasonable to let each function consist of the nominal shape modified by small perturbations. We will take the perturbations to be members of the following uncertainty set:

$$\begin{aligned} \tilde{h}_k(x_l - x_k, y_l - y_k) &= [1 + \delta_k(\cdot,\cdot)]\, h_k(\cdot,\cdot) \\ &\quad -\Delta \le \delta_k(\cdot,\cdot) \le \Delta \quad \forall\, k,l \end{aligned} \tag{15}$$

Typical values of the uncertainty set's magnitude bound are $\Delta \approx 0.05 - 0.2$.

Substituting Eqn (15) into (4) gives the following perturbed model:

$$d = (H + \delta H)\, u + d_0, \tag{16}$$

where again $H = \{h_k(x_l - x_k, y_l - y_k)\}$ and $\delta H = \{\delta_k(\cdot,\cdot)\, h_k(\cdot,\cdot)\}$, with detailed structure depending on the ordering scheme used to index the cells.

By choosing a specific member from the uncertainty set, namely $\delta_k(x_l - x_k, y_l - y_k) = \Delta$, $-\infty < k,l < \infty$, it is easy to see that the additive perturbations in (16) are bounded by

$$\sigma_{\max}(\delta H) \le \Delta \cdot \sigma_{\max}(H) \tag{17}$$

where $\sigma_{\max}(M)$ is the usual maximum singular value of matrix M.

Various Monte Carlo experiments have been performed on models of the form (16) with identical nominal influence functions, regular cell spacing, and modest overall dimensions (e.g., spatially invariant systems with dimension $N < \infty$). Using randomly selected perturbations from the uncertainty set, statistically independent and uniformly distributed for each cell, we searched for particularly 'bad' perturbations (in a sense of the singular value $\sigma_{\max}(\delta H)$ in (16) being large). These experiments indicate that the 'bad' perturbations tend to be similar for all cells and to take their values at extremes of the uncertainty set, $\delta \approx \pm\Delta$. Indeed, when the perturbations are restricted to be identical for all cells and to take values at extremes, then bad ones emerge in the experiments much more frequently. These numerical results suggest that perturbations for spatially invariant systems may be treated as spatially invariant themselves, and that they can be assumed to take only extreme values. Under these conditions, the uncertainty set in Eqn (15) can be simplified to

$$\begin{aligned} \tilde{h}(m\Delta x, n\Delta y) = \tilde{h}_{mn} &= h_{mn} + \delta_{mn}\, h_{mn}, \\ \delta_{mn} &= \pm\Delta, \quad -\infty < m,n < \infty, \end{aligned} \tag{18}$$

where again, the original index k has been replaced by the double index m,n, referencing cells on a uniform 2-D grid.

Following standard temporal dynamic system theory, let the norm of an influence function be defined as the supremum over spatial frequencies of its transform, i.e., $\|h\| = \sup_{\xi,\lambda} |h^*(v,w)|_{v=\exp(j\xi\Delta x),\ w=\exp(j\lambda\Delta y)}$. Then, by selecting the perturbation $\delta_{mn} = \Delta$, $\forall\ m,n$, it is easy to see that the additive perturbations in Eqn (18) are bounded by

$$\|\{\delta_{mn} h_{mn}\}\| \le \Delta\, \|h\| \tag{19}$$

Also, it is evident that for this selected perturbation its peak magnitude occurs at the same frequencies as the peak of $h^*(v,w)$. Moreover, other perturbations can be constructed that have the same norm, but have their peak at different frequencies. For example, if the peak of $h^*(v,w)$ happens to occur at $\xi = \lambda = 0$ (spatial DC), then the modulation $\delta_{mn} = \Delta(-1)^{m+n}$, $\forall\ m,n$ moves the peak to the half-Nyquist frequencies. Other modulations can be chosen to move peaks to other frequencies, although not all frequencies are available because modulation alternatives are discrete. The net consequence is that the uncertainty set for spatially invariant systems, Eqn (18), can be replaced with little conservatism by a simpler set of additive perturbations with constant magnitude across all spatial frequencies. With this substitution, the perturbed form of Model (13) becomes

$$\begin{aligned} d^*(v,w) = \frac{h^*(v,w) + \varepsilon}{s + a^*(v,w)} u^*_{cmd}(v,w) \;+\; d_0(v,w) \\ |\varepsilon| \le \Delta\, \|h\|, \quad \forall\ v,w \end{aligned} \tag{20}$$

As a final observation, note that for spatially invariant arrays with very large size N, both $\sigma_{\max}(H)$ and $\|h\|$ are operator norms of the same convolution operation. Hence, Eqn (17) and Eqn (19) express the same bound on uncertainties. And, since perturbations exist for (19) that have their peaks at many spatial frequencies, we must also expect that perturbations exist for (17) that have their maximum singular value along many singular-vector directions of matrix H, and specifically along its weakest direction corresponding to $\sigma_{\min}(H)$.

IV. Control Design Using Transform Models

Combining (20) and (14) gives the following closed loop transfer functions:

Closed loop errors (sampled deformations):

$$e^* = (r^* - d^*) = \frac{s + a^*}{s + a^* + (h^* + \varepsilon)\, k^*}(r^* - d_0^*) \tag{21}$$

Closed loop actuator displacements:

$$u^* = \frac{k^*}{s + a^* + (h^* + \varepsilon)\, k^*}(r^* - d_0^*) \tag{22}$$

Closed loop errors (continuous deformations):

$$\begin{aligned} \tilde{d} &= \tilde{h} u^* + \tilde{d}_0 \\ \tilde{e} &= \tilde{r} - \tilde{d} = \tilde{r} - \tilde{d}_0 - \frac{\tilde{h} k^*}{s + a^* + h^* k^*}(r^* - d_0^*) \end{aligned} \tag{23}$$

For notational simplicity, the dependence of variables and parameters on spatial frequencies v, w has been suppressed in these equations.

Equations (21)–(23) exhibit several basic features of closed-loop deformation control. For example, Eqn (21) shows that all spatially sampled deformation errors can be reduced to zero in temporal steady state (i.e., when $s = 0$) as long as $a^* = 0$ (i.e., for pure integral action). However, for these same conditions, Eqn (22) shows that the displacements of actuators u^* will be

proportional to $1/(h^*+\varepsilon)$. Therefore, if $h^*+\varepsilon$ turns out to be zero or very small at some combination of spatial frequencies, these displacements will be excessive. Non-zero integrator leakage terms $a^* > 0$ are necessary at such frequencies to alleviate this problem. This corresponds to the high-frequency roll-off required of the control loop in classical control, only this roll-off occurs in the spatial frequency.

Also, Eqn (23) shows that even when spatially sampled deformations from (21) are zero in steady state, their continuous counterparts are not necessarily zero. In fact, for wide-band references and disturbances, $(\tilde{r}-\tilde{d}_0) = (r^*-d_0^*) = 1$, we get $\tilde{e} = 1-\tilde{h}/h^*$. This error expresses the (necessarily) limited ability of the system's continuous actuator influence functions to interpolate between spatial samples. However, it turns out that some influence functions do a better job of interpolating than others. Hence, the shape of these functions is an important design consideration for the basic deformation mechanism of the actuator/sensor array. Note that matrix models (4) and (16) provide no similar direct way to look at the inter-sample behavior of deformations.

Given that the control law has been selected to be the fixed-form structure in (14) , our control design problem reduces to choosing the structure's parameters, $k^*,\ a^*$, such that selected closed-loop design objectives are satisfied. We will concentrate on the following objectives:

Objective (1): Robust stability: This requires characteristic equations to remain non-zero, i.e.,

$$|s + a^* + (h^*+\varepsilon)k^*| \quad \geq \quad p_0^* \tag{24}$$

Objective (2): Robust small deformation errors: This requires transfer functions in Eqn (21) to remain below specified error bounds, i.e.,

$$\left|\frac{s+a^*}{s+a^*+(h^*+\varepsilon)\,k^*}\right| \quad \leq \quad W_1(s,p_1^*), \tag{25}$$

where $W_1(s,p_1^*)$ corresponds to the usual frequency-weighted error bound from standard control design practice. This bound typically calls for small errors at low temporal frequencies, and it permits large errors ($\approx$ unity) at frequencies beyond the temporal bandwidth. To keep controllers simple, detailed shapes are generally selected to match 'natural' shapes of the temporal loop. For instance, letting $W_1(s,p_1^*) = \left|\frac{s+a^*}{s+p_1^*}\right|$ leads to the following robust performance specification:

$$\left|\frac{1}{s+a^*+(h^*+\varepsilon)\,k^*}\right| \quad \leq \quad \left|\frac{1}{s+p_1^*}\right| \tag{26}$$

Note that this choice of $W_1(s,p_1^*)$ shares the 'natural' numerator of the plant but imposes minimum temporal bandwidths specified by parameter p_1^*.

Objective (3): Robust bounded actuator displacements: This requires transfer functions in Eqn (23) to remain below specified displacement bounds, i.e.,

$$\left|\frac{k^*}{s+a^*+(h^*+\varepsilon)\,k^*}\right| \quad \leq \quad W_2(s,p_2^*) = \frac{1}{p_2^*}$$

Each of these inequalities must be satisfied for all perturbations $|\varepsilon| \quad \leq \quad \Delta\,\|h\|$, for all temporal frequencies $s = j\omega$, $0 \leq \omega < \infty$, and for all spatial frequencies $v = \exp(j\xi\Delta x)$, $w = \exp(j\lambda\Delta y)$, $0 \leq \xi\Delta x, \lambda\Delta y \leq 2\pi$.

The parameters $p_0^*,\ p_1^*,\ p_2^*$ are closed-loop specifications supplied by the design team. For most systems, all three can be treated as positive constants, requiring uniform closed-loop behavior over all spatial frequencies. However, for systems with very small (or even negative) $h^*+\varepsilon$ in some frequency regions, it is necessary to exclude those regions from Objective (2).

Objectives (1)-(3) have two key properties that make them tractable. First, as mentioned above, because of the symmetry the transform functions h^*, a^* and k^* are real-valued for spatial frequencies on the unit circle. Second, with real-valued transforms, the worst-case perturbations ε are also real-valued, and the left-hand sides of all three design objectives achieve their extremes at $s = 0$ (i.e., at temporal steady state). Hence, the temporal degree of freedom can be removed for the design process. Furthermore, with real-valued transforms, we can clear the denominators of (25)–(26) to produce a set of linear inequalities in the design parameters $k^*,\ a^*$ (see [5]):

$$\begin{aligned} a^*+h^*k^* &\geq p_0^*+\Delta\,\|h\|\,k^* \\ a^*+h^*k^* &\geq p_0^*-\Delta\,\|h\|\,k^* \end{aligned} \tag{27}$$

$$\begin{aligned} a^*+h^*k^* &\geq p_1^*+\Delta\,\|h\|\,k^* \\ a^*+h^*k^* &\geq p_1^*-\Delta\,\|h\|\,k^* \end{aligned} \tag{28}$$

$$\begin{aligned} a^*+h^*k^* &\geq k^*(p_2^*+\Delta\,\|h\|) \\ a^*+h^*k^* &\geq k^*(p_2^*-\Delta\,\|h\|) \end{aligned} \tag{29}$$

These inequalities must again be satisfied for all spatial frequencies, with the exception that frequency regions with small or negative $h^*-\Delta\,\|h\|$ must be excluded from (28).

In general, it will be true that $p_0^* \ll p_1^*$, i.e., the stability robustness specification is a lot weaker than the performance specification. So (28) actually dominates (27) except in the regions where it must be excluded. As a result, (27) and (28) can be combined into a single set of inequalities with bounds $p_0^* \pm \Delta\,\|h\|\,k^*$ inside the excluded regions and $p_1^* \pm \Delta\,\|h\|\,k^*$ outside. With this interpretation, the excluded spatial frequency regions are analogous to the crossover region (and beyond) of classical temporal control loops, where stability robustness is the key design issue, and the included regions are analogous to the in-band active control bandwidth, where robust performance is the key issue.

Finally, note that all three sets of inequalities can be satisfied with sufficiently large integrator leakage terms a^*. Unfortunately, such design choices would destroy the controller's integral action and severely undermine Design Objective (2). Instead, we should attempt to preserve the integral action as much as possible by minimizing the leakage terms. In addition, we should also take care to keep the leakage terms non-negative, because negative terms correspond to open-loop unstable controllers that are difficult to test, verify and commission in the field. Hence, it is prudent to add a minimization criterion and another set of inequalities to the design problem, i.e.

$$\iint\ (W_k^*\,k^* + W_a^*\,a^*)\,d\xi d\lambda \rightarrow \min \tag{30}$$

$$a^* \geq 0 \tag{31}$$

In (30), W_k^*, W_a^* are weighting functions on the transforms of control gains and integrator leakage terms, respectively: W_k^* should be small, just to keep solutions bounded, while W_a^* should seriously penalize the leakage terms.

Note that (30) provides a linear optimization criterion for design parameters $k^*,\ a^*$ that are otherwise constrained by linear inequalities (27)–(29) and (31) on the spatial frequency domain. Hence, by gridding the domain and expressing the inequalities at each grid point, linear programs (LPs) can be used to solve the design problem.

It is important to recognize that the use of LPs is not enabled merely by the specific choice of design objectives used above. LPs can in fact capture a much wider range of specifications. For example, in the present modeling/design setup we have assumed that maximum temporal bandwidths are well below the first resonance mode ω_0 of the surface. This assumption can be enforced explicitly by including another inequality analogous to (28) that bounds maximum bandwidths, e.g.,

$$[a^* + h^* k^*] \quad \leq \quad p^*_{1\,\max} = 0.5\varsigma_0\omega_0 \tag{32}$$

With different values of $p^*_{1\,\max}$, such constraints can also enforce bandwidth limitations imposed by other phenomena, such as maximum digital sampling rates of the control hardware or time delays in the surface deformation sensing scheme and/or the communications architecture.

Another example of additional LP-constraints comes from specifications on the controller's temporal steady state error. Ideally, with no integrator leakage, steady state errors at cell locations are zero. However, when leakage is non-zero, steady state errors are also non-zero. In fact, they are given explicitly by $a^*/(a^* + h^*k^*)$. So, in light of the optimization criterion (29), it follows that steady state errors are automatically minimized, in a weighted average sense, by the LP solution. Nevertheless, it may still be desirable to specify explicit constraints on these errors, i.e.

$$\begin{aligned} \frac{a^*}{a^* + h^*k^*} &\leq p_3^* \\ a^* &\leq p_3^*(a^* + h^*k^*) \end{aligned} \tag{33}$$

Finally, it is important to note that once the design parameters are obtained as solutions of LPs, the fact remains that they correspond to actuator/sensor arrays with infinite spatial extent. Formal methods to assure that these solutions also work for finite arrays remain subjects of research. Meanwhile, only brute-force methods of verification are available. These consist of building a series of successively larger finite array models in the form (16) with controller (14) and with $N = N_0 < N_1 < N_2 < \ldots < N_m$, where the largest dimension is limited by computing resources and budgets available to the design team. Closed-loop properties of this series can then be evaluated, and hopefully, they can be shown to converge as N increases. If necessary, the parameters $k^*,\ a^*$ of cells near the array's boundaries can be fine-tuned to improve closed-loop behavior. These steps are illustrated in the design example below.

V. Design Example

We illustrate the above theoretical construction of transform-based design methods with an abstracted example from a proposed large flexible space reflector application [6]. This reflector consists of an active membrane of many cells, each with adjustable thickness, so that it can compensate for local deformation errors of its non-rigid supporting structure. The cell arrangement is hexagonal, as illustrated in Figure 2. Starting with a single hexagonal central cell at the origin of the reflector, the total arrangement consists of many rings of other hexagonal cells around the center.

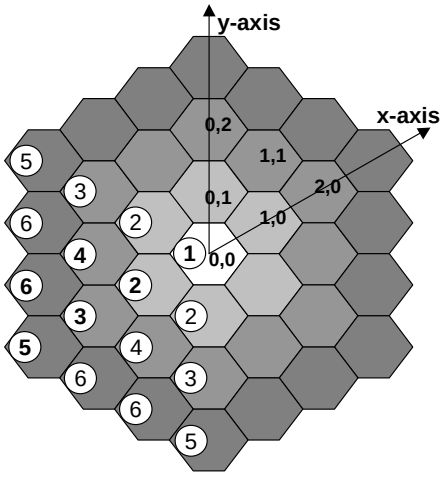

Fig. 2. Design Example with Hexagonal Array

The actuator influence function, the control influence function, and the integrator leakage function for this cell arrangement are assumed to be hexagonally symmetric. This means that several cells share the same function value. The central cell, corresponding to the actuator/controller location in the overall reflector grid, has function parameter value f_1, its first-neighbor surrounding ring of six cells has function parameter value f_2, its second-neighbor ring of twelve cells has parameter values f_3 and f_4, etc. This indexing scheme is illustrated by the circled numbers in Figure 2.

A representative actuator influence function for the reflector is shown in Figure 3. The two-dimensional spatial transform of this pulse response is shown in Figure 4, both as a 'level curve representation' (contour plot) on the spatial frequency domain and as a 'radial curve representation' showing magnitudes along spatial frequency rays covering the frequency domain in 15-degree radial increments. The latter representation is very appealing for control engineers trained in classical frequency response analyses. In particular, it is evident from the radial curves that the influence function provides adequate gain at spatial frequencies below ≈1.5 radians/distance along all radial directions. However, its gain is very low beyond that frequency, recovering only near the spatial sampling frequencies, e.g. at $(\xi, \lambda) = (2\pi, 0), (2\pi, 2\pi)$, and $(0, 2\pi)$, (e.g., as we approach 2π along the 0, 45, and 90-deg rays). The recovery of gain near the sampling frequencies is, of course, a result of the periodicity of discrete transforms in two dimensions. Specifically, the transforms repeat themselves in

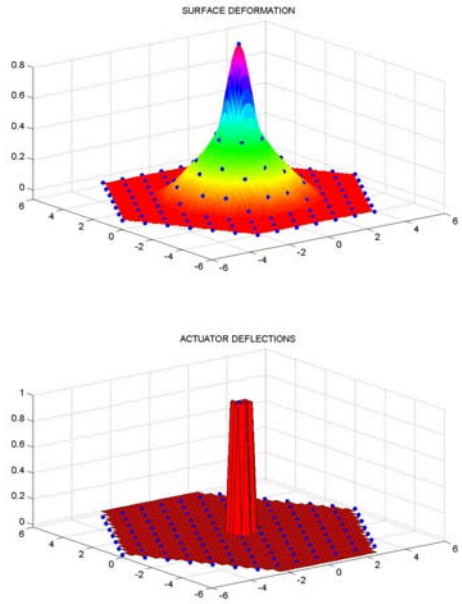

Fig. 3. Spatial Pulse Response. Pulse Response of the Surface Deformation - Upper Plot. Actuator Bump - Lower Plot

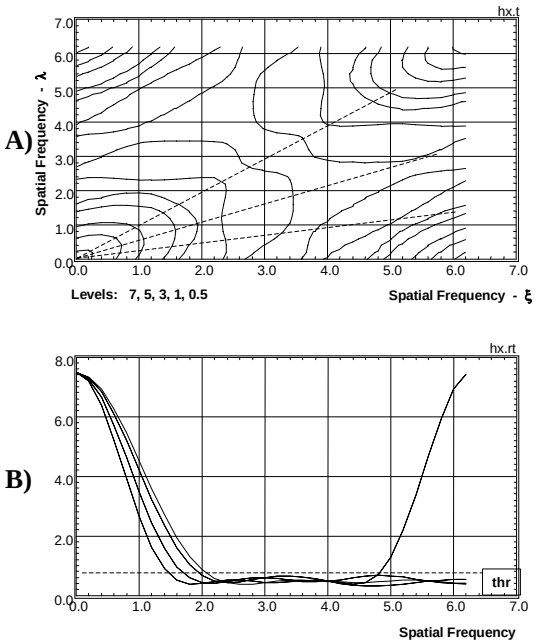

Fig. 4. Spatial Frequency Response, h_x^*. A) Level Curve Representation; B) Radial Curve Representation (15-degree increments)

each consecutive $2\pi \times 2\pi$ square. They also exhibit symmetry within each square. Namely, if we divide the square into four equal sub-squares, then the upper right sub-square is the mirror image of the lower left one, and the upper left sub-square is the mirror image of the lower right one (this is evident in the level curves of Figure 4). This pattern of symmetry is analogous to the symmetry of 1D-transforms, where the function above the half-sample (Nyquist) frequency π is the mirror image of the function below π. Its significance is that design and analyses of 2D-transforms must examine either the full $2\pi \times 2\pi$ square or at least the sub-domains $2\pi \times \pi$ or $\pi \times 2\pi$. Examining only the lower left $\pi \times \pi$ sub-square is not adequate! With this important side observation, the characteristics shown in Figure 4 suggest that the in-band region of our control designs should cover approximately 0-1.5 r/d radially around each of the four corners of the $2\pi \times 2\pi$ square, and that all other frequencies should be considered out-of-band. (A precise definition of the boundary between these regions is determined by the 'in-band threshold' parameter, as illustrated below.)

A. One-Ring Controller

LP-derived control parameters for the system in Figures 3–4 are shown in Figure 5. These parameters correspond to a 'one-ring design', meaning that the control law for each cell was constrained to use only its own local measurements plus measurements from one ring of cells immediately surrounding it (i.e., data from six immediate neighbors).

Design specifications for the controller were the following:

Robust stability: $p_0^* = 0.1$
Robust performance: $p_1^* = 1.0$
Uncertainty level: $\Delta = 0.05$

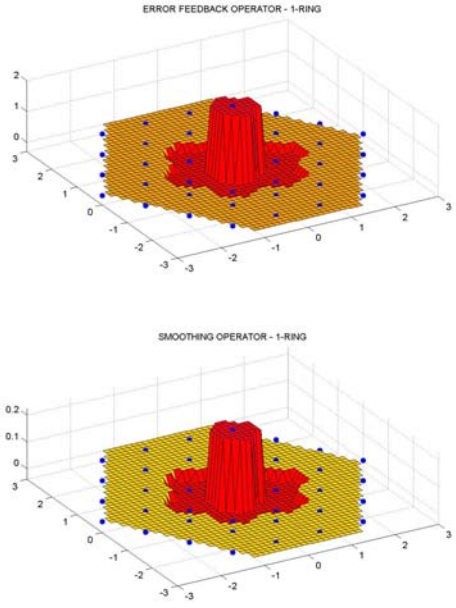

Fig. 5. Feedback Operators in One-Ring Design. Upper Plot: Control Influence Operator, $k = \{2.294, -0.358\}$. Lower Plot: Integrator Leakage Operator, $a = \{0.081, -0.014\}$. The two numbers given here for each of the operators k and a correspond to the cell-ordering scheme in Figure 2

In-band threshold: $h^* - \Delta \|h\| \geq 0.1 \|h\|$
Maximum bandwidth: $p^*_{1\max} = 3$
Minimization Weights: $W^*_k = 10^{-6}, \quad W^*_a = 1.0$
Spatial frequency domain: $(2\pi \times 2\pi)$ rad, 10×10 grid

Spatial frequency domain properties of the one-ring design are shown in Figures 6. Figure 6A gives a radial curve representation of closed loop temporal bandwidths, as compared against the robust performance spec, p^*_1, the robust stability spec, p^*_0, and the maximum bandwidth constraint, $p^*_{1\max}$. Figure 6B gives a similar representation of closed loop steady state error. Note that all specifications are satisfied. Furthermore, from Figure 6B, the integrator leakage terms are small in-band, and they rise out-of-band to assure stability robustness in the presence of uncertainty Δ.

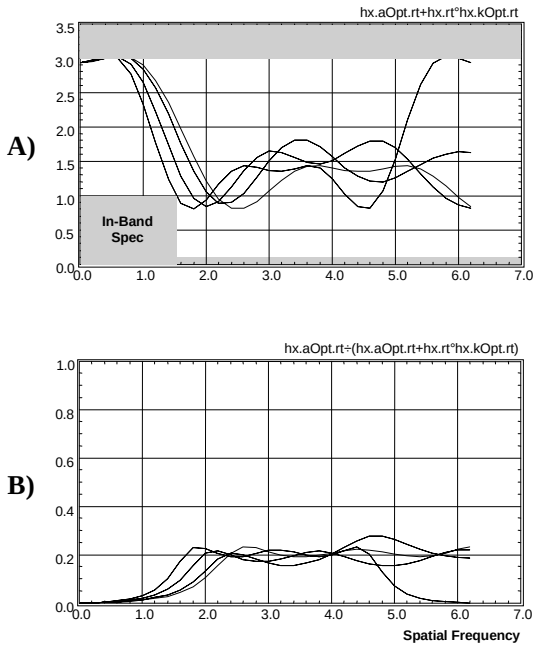

Fig. 6. Spatial Frequency Domain Properties of the One-Ring Solution. A) Temporal Bandwidth, $a^* + k^* h^*$, Radial Curve Representation (15 increments); B) Steady State Error, $a^*/(a^* + k^* h^*)$, Radial Curve Representation

Temporal properties of the one-ring solution are illustrated in Figures 7, 8. These figures contains time simulations of initial condition pulse responses, i.e. at $t = 0$, $u_{00}(t) = 1$, $u_{mn}(t) = 0$ otherwise. First, Figure 7 shows surface deformations and actuator deflections for a 30-ring array at $t = 0$. Figure 8 then shows the surface deformations and actuator deflections that have evolved at $t = 5$. The simulation confirms that the closed loop system is stable for a finite-dimensional array.

Figure 9 shows time responses of the same one-ring controller but for increasingly larger array dimensions. This confirms that temporal properties converge (at least qualitatively) as arrays grow large. Hence, the controller is scalable to very large array dimensions.

Note that initial condition responses include no external disturbances, i.e. $d_0(t) \equiv 0$, so all simulations satisfy $d(t) \to 0$, and $u(t) \to 0$. Simulations with non-zero disturbances do not have this property because high- spatial-frequency disturbance components are not removed completely (Figure 6B). This

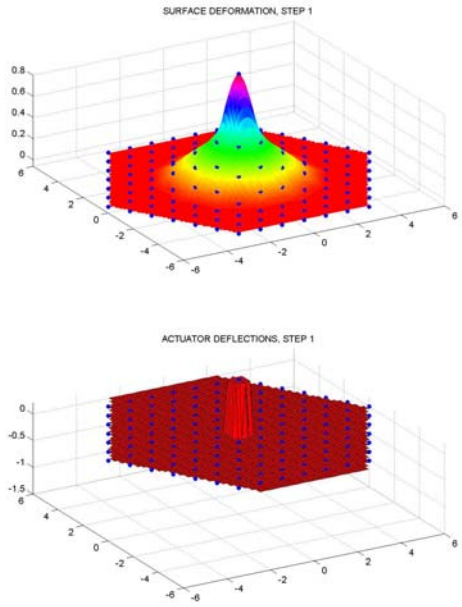

Fig. 7. Temporal Properties of the One-Ring Solution: Pulse Compensation, the system at $t = 0$. Upper Plot: Surface Deformations. Lower Plot: Actuator Deflections.

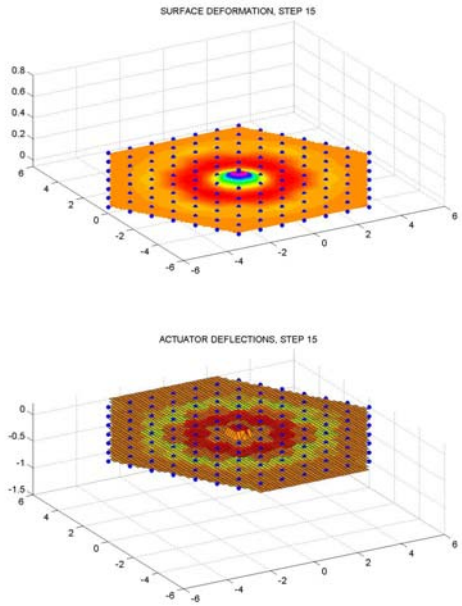

Fig. 8. Temporal Properties of the One-Ring Solution: Pulse Compensation, the system at $t = 15$. Upper Plot: Surface Deformations. Lower Plot: Actuator Deflections.

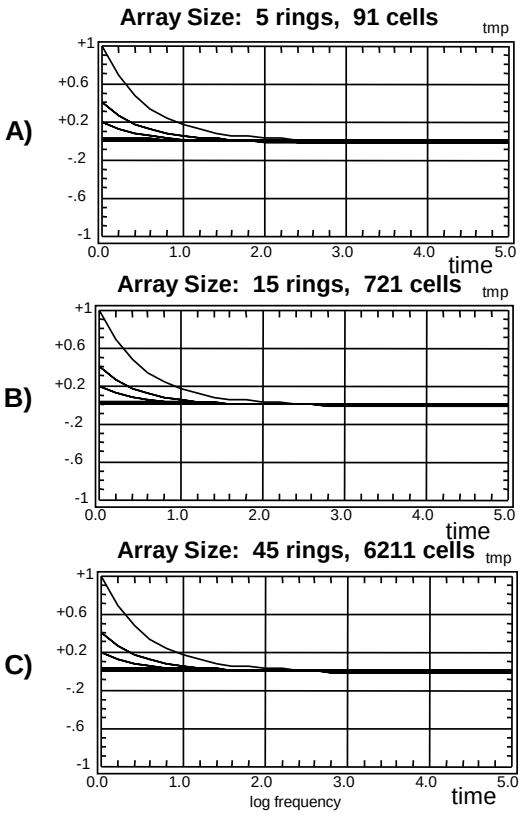

Fig. 9. Temporal Properties of the One-Ring Solution. Initial Condition Pulse Responses. Growing Array Size, y-Axis Cross-Section

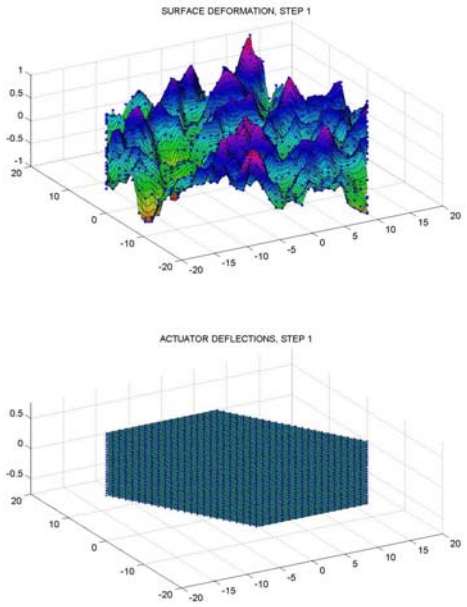

Fig. 10. Temporal Properties of the One-Ring Solution: Random Initial Condition Compensation, the system at $t = 0$. Upper Plot: Surface Deformations. Lower Plot: Actuator Deflections

is illustrated in Figures 10 and 11 which show simulation results for spatially smoothed random disturbances. Note that the closed loop system reduces uncontrolled disturbance levels of 0.32 (2-sigma along the y-axis cross-section) down to 0.018, an approximate 18:1 improvement factor.

B. Two-Ring Controller

Similar results for a second controller design are shown in Figures 12 through 16. This second controller is a so-called 'two-ring design', meaning that the control law for each cell was constrained to use its own local measurements plus measurements from two rings of cells immediately surrounding it (i.e., data from eighteen neighbors, each no more than two cells away). The LP-derived parameters for this case are shown in Figures 12, corresponding to the same specifications used for the above discussed one-ring design. Frequency domain properties of the two-ring solution are shown in Figures 13 and 14.

Results of temporal simulations of the closed loop system are shown in Figure 15 (pulse responses) and Figure 16 (random disturbance responses).

The two-ring design meets all robust performance, stability robustness, and maximum bandwidth constraints. This controller was compared to a one-ring design (control for each cell uses only this cell data and data for one ring of nearest neighbours). The two-ring was found to be also superior to the one-ring design, because its steady state errors are lower

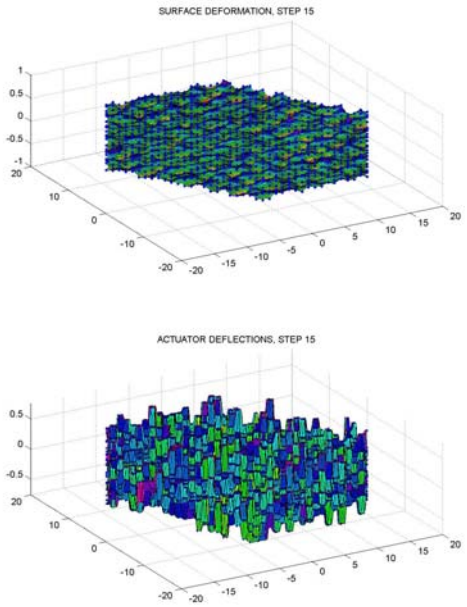

Fig. 11. Temporal Properties of the One-Ring Solution: Random Initial Condition Compensation, the system at $t = 15$. Upper Plot: Surface Deformations. Lower Plot: Actuator Deflections

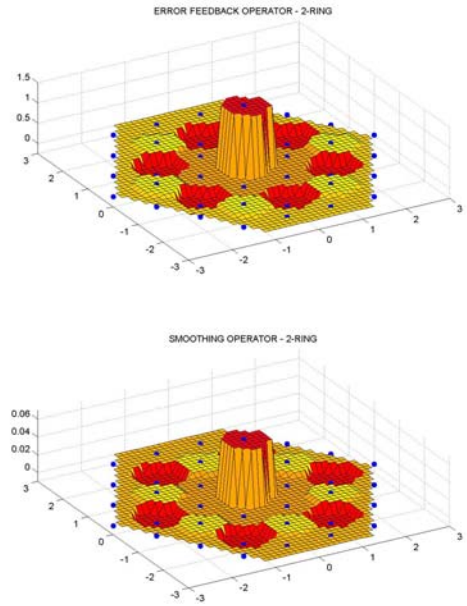

Fig. 12. Feedback Operators in Two-Ring Design . Upper Plot: Control Influence Operator, $k = \{1.474, -0.032, 0.053, -0.244\}$. Lower Plot: Integrator Leakage Operator, $a = \{0.062, -0.002, -0.010, 0.002\}$. As before, the four numbers for k and a correspond to the cell-ordering scheme in Figure 2.

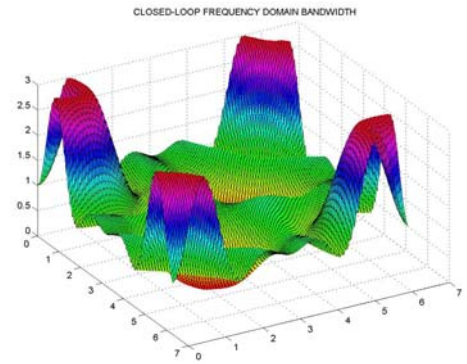

Fig. 13. Temporal Bandwidth, $a^*(\lambda,\xi) + k^*(\lambda,\xi)h^*(\lambda,\xi)$, in Spatial Frequency Domain for the Two-Ring Solution.

on average. This is evident in Figure 14A, which shows lower average errors than those in the corresponding Figure 6. The closed loop control results in Figure 16 show the disturbance level of 0.5718 (quadratic variation of the error in the end of the simulation). This is an approximate 2:1 improvement factor compared to the disturbance level 1.0942 obtained for one-ring design.

It is also evident from Figures 13, 14, that the designed two-ring controller exhibits two localized spatial frequency regimes (near $(\xi,\lambda) = (2,4)$ and $(4,2)$, where steady state errors are nearly 80% (e.g., very little disturbance rejection occurs there). Note that these are 'super-Nyquist' frequencies, outside of the lower left $[0,\ \pi] \times [0,\ \pi]$ sub-square, and a sampled system cannot be expected to yield good performance

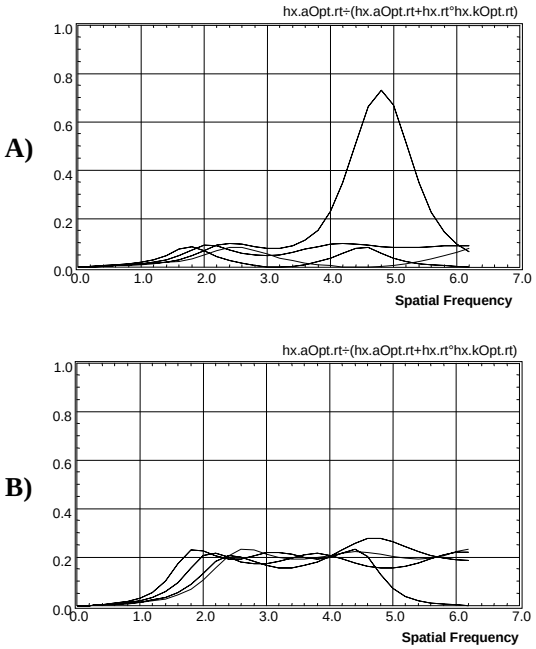

Fig. 14. Spatial Frequency Domain Properties of the Two-Ring Solution. A) Temporal Bandwidth, $a^* + k^*h^*$, Radial Curve Representation (15^o increments); B) Steady State Error, $a^*/(a^* + k^*h^*)$, Radial Curve Representation.

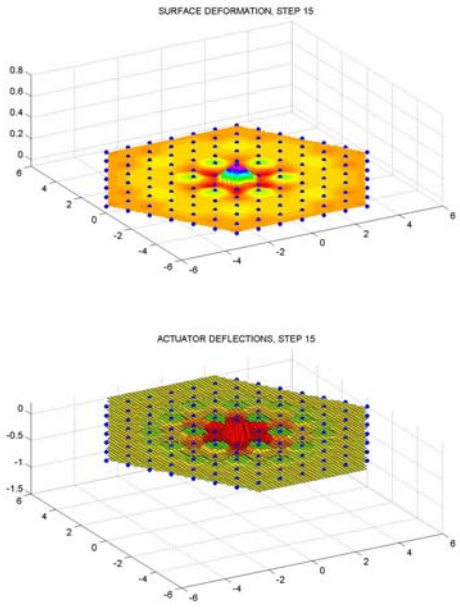

Fig. 15. Temporal Properties of the Two-Ring Solution: Pulse Compensation, the system at $t = 15$. Upper Plot: Surface Deformations. Lower Plot: Actuator Deflections

at these frequencies. Nevertheless, we must still assure the required level of stability robustness, p_0^*, is satisfied.

This is confirmed in Figures 13, 14.

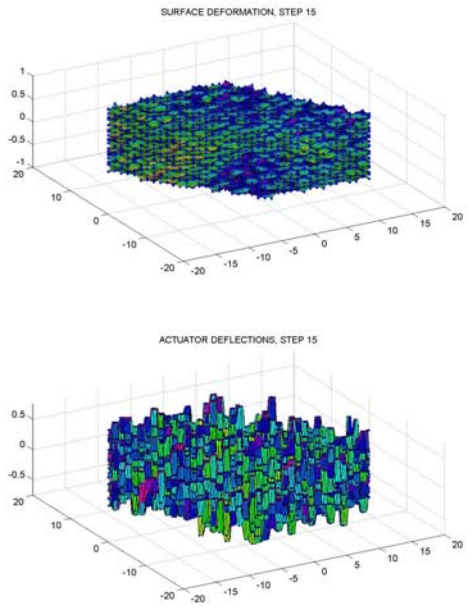

Fig. 16. Temporal Properties of the Two-Ring Solution: Random Initial Condition Compensation, the system at $t = 15$. Upper Plot: Surface Deformations. Lower Plot: Actuator Deflections

VI. Conclusion

This paper has developed a classically-motivated design methodology for distributed localized control laws of very large actuator/sensor arrays. Standard PI-compensation, plus lags and/or notch-filters, are used to deal with temporal dynamics in each actuator channel. Scalability to very large array sizes is achieved by imposing spatially localized fixed-form constraints on the control law structure. In this setup, the entire spatial-temporal design model can be transformed, via Laplace transforms in time and 2D discrete Fourier transforms in space, to produce a family of dynamic systems whose closed loop characteristics can be subjected to standard classical control-engineering specifications, including stability, performance, and robustness. These specifications can be satisfied for all members of the family by solving linear programs to find parameters of the fixed-form structure. The veracity of this methodology has been illustrated with a design example loosely resembling an actively controlled reflector whose local deformations are controlled by a hexagonal array of actuator/sensor cells. We have designed and compared two controllers for this example – a one-ring design where only nearest neighbors are used in the fixed- form control law and a two-ring design where the first and second neighbors are used. Both designs yield good performance. The two-ring design is generally superior to the one-ring design because it delivers significantly smaller average steady state errors.

References

[1] Bamieh, B., Paganini, F., and Dahleh, M. "Distributed control of spatially-invariant systems," *IEEE Trans. on Automatic. Contr.*, Vol. 47, No. 7, 2002, pp. 1091 -1107.

[2] Bose, N.K. *Applied Multidimensional Systems Theory*, Van Nostrand Reynhold, 1982

[3] D'Andrea, R., and Dullerud, G.E., "Distributed control for spatially interconnected systems," *IEEE Trans. on Automatic Control*, Vol. 48, No. 9, 2003, pp. 1478–1495.

[4] Gorinevsky, D., and Stein G., "Structured uncertainty analysis of robust stability for multidimansional array systems," *IEEE Trans. on Automatic Control*, Vol. 48, No. 9, 2003, pp. 1557–1568.

[5] Gorinevsky, D., Boyd, S., and Stein G., "Optimization-based tuning of low-bandwidth control in spatially distributed systems," *American Control Conference*, Denver, CO, June 2003.

[6] Gorinevsky, D., Hyde, T., and Cabuz, C. "Distributed shape control of lightweight space reflector structure," *IEEE Conference on Decision and Control*, Vol. 4, pp.3850 -3855, Orlando, FL, December 2001.

[7] MacMartin, D.G., "Local, hierarchic, and iterative reconstructors for adaptive optics," *J. Opt. Soc. Am. A*, Vol. 20, No. 6, 2003, pp. 1064–1093.

[8] Stewart, G.E., Gorinevsky, D., and Dumont, G.A. "Two-dimensional loop shaping," *Automatica*, Vol. 39, No. 5, 2003, pp. 779-792.

[9] Stewart, G., Gorinevsky, D., and Dumont, G. "Feedback controller design for a spatially distributed systems: The paper machine problem," *IEEE Trans. on Control Systems Technology*, Vol. 11, No. 5, 2003, pp. 612–628.

[10] Kilkarni, J.E., D'Andrea, R. "Application of distributed control technique to an adaptive secondary mirror," *American Control Conf.*, Denver, CO, June 2002

[11] Tikhonov, A.N., and Arsenin, V.Ya. *Solutions of Ill-Posed Problems*. Halsted Press, Washington, 1977.

[12] Vorontsov, M.A., and Carhart, G.W., Cohen, M., and Cauwenberghs, G. "Adaptive optics based on analog parallel stochastic optimization: analysis and experimental demonstration," *J. Opt. Soc. Am.*, Series A, Vol. 17, No. 8, August 2000

PLACE PHOTO HERE

Dimitry Gorinevsky (M'91–SM'98) is a Senior Staff Scientist with Honeywell Labs and a Consulting Professor of Electrical Engineering at Stanford University. He received a Ph.D. from Moscow Lomonosov University and a M.Sc. from the Moscow Institute of Physics and Technology. He held research, engineering, and academic positions in Moscow, Russia; Munich, Germany; Toronto and Vancouver, Canada. His interests are in decision and control systems applications across many industries. He has authored a book, more than 130 reviewed technical papers and a dozen patents. Dr. Gorinevsky is an Associate Editor of IEEE Transactions on Control Systems Technology. He is a recipient of Control Systems Technology Award, 2002, and Transactions on Control Systems Technology Outstanding Paper Award, 2004, of the IEEE Control Systems Society.

PLACE PHOTO HERE

Gunter Stein (S'66–M'69–F'85) is a Chief Scientist (ret) of Honeywell Technology Center (now Honeywell Labs). He received a PhD in EE from Purdue University in 1969. His technical specialization is in systems and control, particularly aircraft flight controls (fighters, transports, and experimental vehicles), spacecraft attitude and orbit controls, and navigation systems for strategic, tactical, and commercial applications. From 1977 to 1997, Dr. Stein also served as Adjunct Professor in EE and CS at MIT, teaching control systems theory and design. He is also active in the development of computer aids for control system design. Dr. Stein was elected fellow of the IEEE in 1985, was awarded the IEEE Control System Society's first Hendrick W. Bode Prize in 1989, was elected to the National Academy of Engineering in 1994, and was awarded the IFAC's Nathaniel Nichols Prize in 1999.